Ion Temperature Measurements of L-mode Filaments in MAST by Retarding Field Energy Analyser

S Y Allan[1], S Elmore[1], G Fishpool[1], B Dudson[2], the MAST Team[1] and the EUROFusion MST1 Team[3]

[1] CCFE, Culham Science Centre, Abingdon, Oxon, OX14 3DB, UK
[2] York Plasma Institute, Department of Physics, University of York, Heslington, York, YO10 5DD, UK
[3] http://www.euro-fusionscipub.org/mst1

E-mail: scott.allan@ccfe.ac.uk

August 2015

Abstract. Retarding field energy analysers (RFEAs) have been used to compare the ion temperature (T_i) of large plasma filaments with the background plasma (composed of small scale filaments) at the midplane and divertor target in L mode discharges in the Mega Amp Spherical Tokamak (MAST). At low densities, at the midplane and divertor, at distances from 2 to 4cm from the separatrix the temperature of ions in large filaments was found to be 2 to 3 times larger than the background plasma. At the midplane, the electron temperature for both large filaments and background plasma was around 3 to 7 times smaller than the ion temperature and had a flat profile across the scrape off layer (SOL). At higher densities, at the midplane and divertor, both the filament and background ion temperatures were smaller than at low density. At the midplane, the filament and background ion and electron temperature profiles across the SOL were relatively flat and of comparable magnitude, ranging in temperature from 5 to 25eV.

Submitted to: *Plasma Phys. Control. Fusion*

1. Introduction

In future nuclear fusion devices such as ITER and DEMO, where hundreds of megawatts of power will be generated, the deposition of energy on first wall and divertor surfaces will be a major factor in determining the lifetime of the machine. The exhausting of a significant part of this power will be done through the scrape off layer (SOL) which is defined as the region where magnetic field lines intersect with solid surfaces. In the SOL, particles and energy can be transported in directions both parallel and perpendicular to magnetic field lines. While parallel transport directs particles and energy to regions

designed to tolerate high power loads, perpendicular transport results in interactions with less robust materials and potential wall damage.

Plasma behaviour in the SOL of tokamaks is driven by turbulence in the edge region where density and temperature gradients are large. This generates intermittent structures of increased density and temperature known as filaments (or blobs) which extend along the magnetic field lines [1]. Within these regions, a charge separation of ions and electrons occurs due to the curvature and non-uniformity of the magnetic field generating a $\mathbf{B} \times \nabla \mathbf{B}$ drift. This generates an electric field within the filament which results in the filament being subjected to an $\mathbf{E} \times \mathbf{B}$ force which drives the filament radially outward across the SOL. Filaments in the SOL have been studied extensively in tokamaks and reviews exist for both experimental measurements [2, 3] and for theory and simulations [3, 4]. Filaments occur in both L-mode and H-mode during edge localised modes (ELMs) [5] and during inter-ELM periods [6]. Filament lifetimes range from 40-60μs in L-mode plasmas, from 50-120μs during inter-ELM periods and from 100-180μs in ELMs [5].

Experimental measurements of filaments have been made using electrical probes, fast camera imaging, microwave reflectometry, laser scattering and heavy ion beam probes [2]. Electrical probes have the advantage of being able to provide localised measurements of filament density, temperature, potential and velocity at time resolutions of tens of μs. The main limitations of probes are the perturbation they can cause to the plasma and the recycling of ablated probe material which can affect plasma properties. Electrical probes have been used to study filaments in a number of tokamaks including Alcator C-Mod [7], ASDEX Upgrade (AUG) [8], DIII-D [9], JET[10, 11], MAST [12], NSTX [13] and TCV [14].

Most electrical probes are Langmuir probes which measure electron temperature (T_e) and density (n_e) and in ion saturation current mode allow data on filament structure and statistics to be accumulated. Conditional averaging of ion saturation current data (selecting peaks above a certain threshold) allows filament statistics to be accumulated. This has shown that the general profile of a filament as it passes over a probe has a full width half maximum of tens of μs with a steep rise and slow decay. Ion saturation current data has shown that positive fluctuations above the mean level dominate the far SOL, an approximately equal number of positive and negative fluctuations occur at the edge velocity shear layer and negative fluctuations dominate inside the velocity shear layer.

A more recent innovation has been the use of retarding field energy analysers (RFEAs) to measure filament ion temperature (T_i). In MAST, ELM ions with energies greater than 500eV have been measured 19cm from the last closed flux surface (LCFS) [15]. In JET, RFEA measurements together with a transient simulation model were used to estimate an ELM filament ion temperature of 100 to 150eV near the limiter radius which was approximately half the pedestal ion temperature [16]. In AUG, a conditional averaging technique similar to that used with Langmuir probes measured ELM filament ion energies as a function of ELM energy and distance from the LCFS [17] with ELM

ion energies of 20-200eV, 35-60mm from the separatrix which was 5-50% of the pedestal T_i. Filament ion temperatures in L-mode plasmas have also been measured in AUG with a T_i of 80-110eV at a distance of 21mm from the separatrix which was 3 to 4 times T_e and 50-70% of the ion temperature at the separatrix [18].

This paper reports on measurements made in MAST L-mode plasmas of ion temperatures in large filaments above a threshold level and background plasma composed of small filaments below the threshold level. Measurements were made using a RFEA mounted on a reciprocating probe (RP) at the midplane and a RFEA at the divertor target. In a previous paper, both RFEAs were used to measure L-mode ion temperatures by averaging over these large filaments and background plasma composed of small scale filaments [19].

This work has been done as part of a study for MAST Upgrade into the role of filaments in the distribution of power and particles onto the divertor nose and into the super-X divertor chamber [20]. While power and heat flux measurements on MAST show fall off lengths of the order of 10 to 25 mm in L-mode [21], fast camera data shows large L-mode filaments can have radial extents of between 50 to 100mm [5]. This indicates that while small filaments transport the majority of particles and power into the near SOL, larger filaments can propagate plasma into the far SOL. The ability of RFEAs to measure both ion and electron temperature make them uniquely suited for the study of filaments and their energies in the SOL. The measurements in this work show that while filament density rapidly drops on length scales of 10-20mm in the SOL, filaments carry ions with relatively high energies into the far SOL to distances of 10 to 40mm from the LCFS. This result is significant as the energy of ions greatly affects the sputtering yields from walls.

Section 2 of this paper describes the experimental set up and method used to obtain filament T_i using the RFEAs. Section 3 gives results from filament and background ion temperature measurements at the midplane and divertor and section 4 draws conclusions from the results obtained.

2. Method

Filament measurements were made in MAST [22] in Ohmic deuterium plasmas with plasma currents of 0.4 and 0.6 MA and line averaged electron densities in the range (1-2.3) x $10^{19}\mathrm{m}^{-3}$. Ion energy measurements were made using RFEAs located at the midplane on a reciprocating probe (RP) system [23] and at the divertor using the Divertor Science Facility (DSF) [24]. The RP allows probes to be moved in and out of the scrape off layer giving measurements as a function of probe position. The DSF is fixed at a radius of R=0.985m but makes measurements as a function of radial distance from the plasma due to the changing magnetic flux of the central solenoid which sweeps the outer strike point over the DSF. The plasma current (I_p) and line averaged electron densities ($\bar{n}_e$) for the shots studied are shown in figure 1 along with the distance of the RFEA from the separatrix ($r - r_{sep}$) during a typical reciprocation. A list of parameters

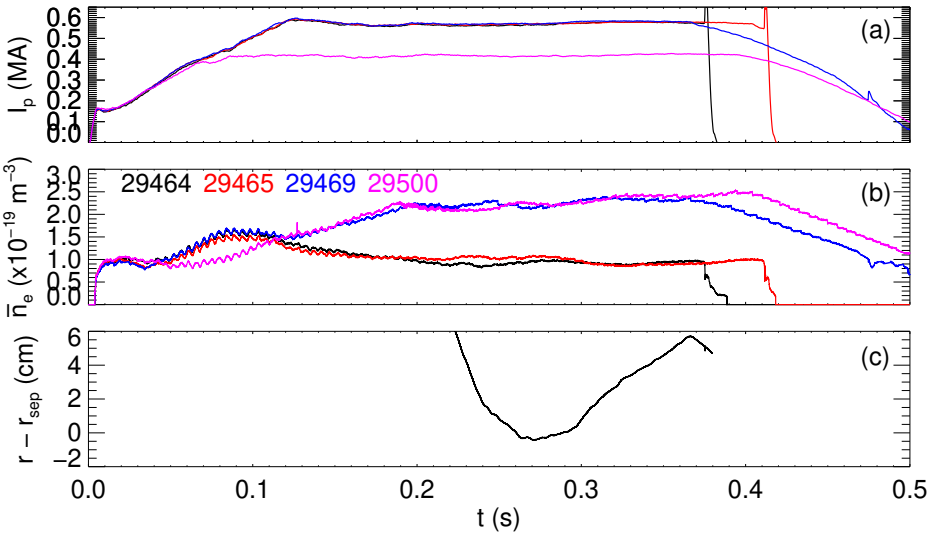

Figure 1. (a) Plasma current (I_p), (b) line averaged electron density ($\bar{n}_e$) and (c) the typical distance of the midplane RFEA inlet aperture from the separatrix ($r - r_{sep}$) for the shots used in this work.

(density (n), plasma current (I_p), toroidal field strength (B_T), q_{95} and Greenwald density fraction (f_{GW})) for the shots studied is given in table 1. All discharges were in a double null configuration.

Table 1. Shot parameters for plasmas studied

n (x10^{19}) (m^{-3})	Shots	I_p (MA)	B_T (T)	$q_{95} \pm 0.5$	f_{GW}
1	29464, 29465	0.6	0.58	6.5	0.22
1	30357	0.6	0.58	7.7	0.22
2	29469	0.6	0.58	6.0	0.44
2	29500	0.4	0.58	7.3	0.67

Both RFEAs consist of a series of electrically biased grids separated by PEEK insulators and mounted inside an electrically grounded graphite shell. The face of the grid stack was aligned so that it was perpendicular to a field line of 30° which was within ±10° of the pitch angles of the shots used. The midplane RFEA is bidirectional and is fitted with grid stacks facing in both directions along the magnetic field line. A detailed description of both RFEAs can be found in reference [19]. A schematic of the grid arrangement and typical voltage profile of the RFEAs is shown in figure 2. Plasma enters the RFEA through a rectangular inlet with an area of 19.1 mm^2. The slit plate is biased at -100V to repel electrons. Grid 1 is swept from 0 to 150V at a frequency of approximately 1kHz to discriminate which energy ions are allowed to pass through to the grounded collector at the rear of the grid stack where the ion current is measured. Grid 2 is biased negatively to minimise the effects of secondary electron emission on ion

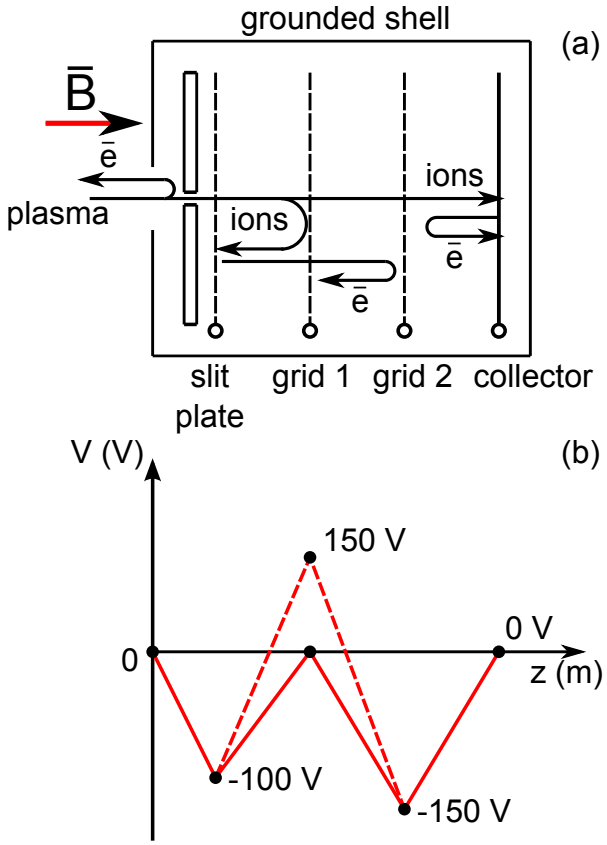

Figure 2. (a) Schematic of the RFEA grid arrangement and (b) typical voltage settings measured with respect to torus ground.

current measurements. In this paper only data from the side of the midplane RFEA facing into the plasma flow, which was assumed to be directed along the field line to the lower divertor, are reported as the signals on this side were larger, making filament identification easier. The DSF RFEA was directed into the plasma flow at the divertor with the front face of the probe perpendicular to the incoming magnetic field lines.

Filaments were detected as spikes in the slit plate ion saturation current trace. For a spike to be considered a filament it was required to have a peak value that was two standard deviations above the mean value over a 5ms interval. As ion saturation current is dependant on density and temperature, the classification of filaments was also dependent on these values. An example of signals from the midplane RFEA are shown in figure 3. The top trace shows the voltages applied to the slit plate and grid 1. Grid 1 was swept to determine ion temperature and the slit plate was swept to determine electron temperature (slit plate sweeping was not used for filaments). Filaments were only recorded when the slit plate voltage was below -90V to ensure only ions were measured. The middle trace shows the slit plate current (I_{sp}). The green dashed line shows the mean of the current and the blue dashed line shows the filament detection threshold equal to the mean plus two standard deviations over the time interval shown. The bottom trace shows the collector current (I_c). In both current traces the peaks

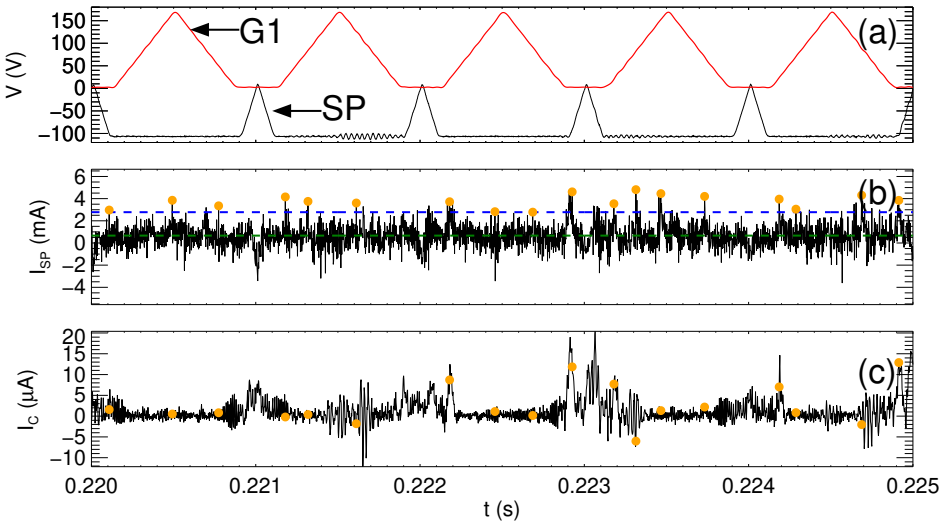

Figure 3. Midplane RFEA signals. (a) Slit plate (SP) and grid 1 (G1) voltage. (b) Slit plate current. The green dashed line shows the mean value and the blue dashed line shows the filament detection threshold of the mean plus two standard deviations. (c) Collector current. Detected filaments are shown in (b) and (c) with orange circles.

identified as filaments are shown by orange circles. The signal in figure 3(b) is made up of filaments of different heights and widths. In this work, filaments with peaks in ion saturation current above the detection threshold were classified as large filaments and signals below the threshold were classified as small background filaments.

The slit plate and collector current density traces for a typical filament are shown in figure 4. In both traces the time resolution of the signals is $2\mu s$. The time axis has been centred around the peak in the slit plate current density. The filament width on the slit plate and collector traces is a function of both the filament size and velocity and as a result is not a good indicator of filament size on its own. The full width at half maximum (FWHM) of the filament on the slit plate was $40\mu s$ which is approximately twice the FWHM of typical filaments measured by RFEA on AUG [18]. The slit plate current density (J_{sp}) was obtained by dividing the slit plate current by the area of the inlet in the graphite shell and the collector current density (J_{coll}) was determined by dividing the collector current by the area of the slit in the slit plate of 0.1mm^2. Both the collector and slit plate current signals for the midplane RFEA were band cut filtered between 23 and 37kHz to remove electrical noise caused by switching of the poloidal field coil power supplies.

The filament ion temperatures were determined using a similar method to that applied to ELMs in reference [25]. As a filament passes over the RFEA, both the density and temperature will change and this will affect the ion current density (J)

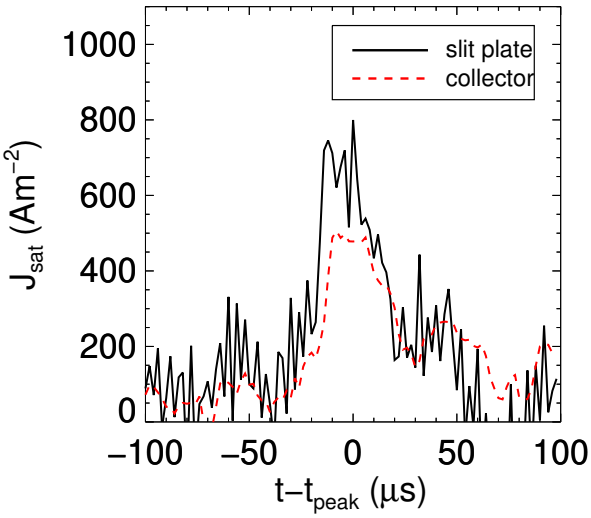

Figure 4. Slit plate and collector current density traces for a typical filament.

which is given by

$$J = env = en\left(\frac{e\left(T_e + T_i\right)}{m_D}\right)^{1/2} \tag{1}$$

where e is the electron charge in C, n is the number density in m^{-3}, v is velocity in ms^{-1}, T_e and T_i are electron and ion temperatures in eV and m_D is the ion mass in kg. The RFEA slit plate measures the total ion current density while the collector measures the ion current density as a function of ion energy due to the potential applied to grid 1 discriminating which ions reach the collector. By normalising the collector current density with the slit plate current density, the effect of density changes during a filament are removed as the normalised signal is expressed as a fraction of the total ion current density at a given time. The average normalised current density ratio (R) is given by

$$R = \frac{\langle J_{coll}\rangle_{fil}}{\langle J_{sp}\rangle_{fil}} = \left(\Delta t_{fil}^{-1}\int_{\Delta t_{fil}} J_{coll}dt\right) / \left(\Delta t_{fil}^{-1}\int_{\Delta t_{fil}} J_{sp}dt\right) \tag{2}$$

where Δt_{fil} was taken to be a $50\mu s$ window centred around the peak of the slit plate current during the filament. Calculations were done using the area under the peak rather than the peak value to reduce the effect of sharp single point spikes which appeared in the probe signals. Filaments pass over the RFEA on timescales of the order of tens of μs which is faster than the ms timescales used to sweep grid 1. As a result, filament ion temperatures were determined by accumulating data from multiple filaments over fixed distance ranges from the separatrix. This method assumes that the ions of different filaments have similar temperature distributions. Assuming that the

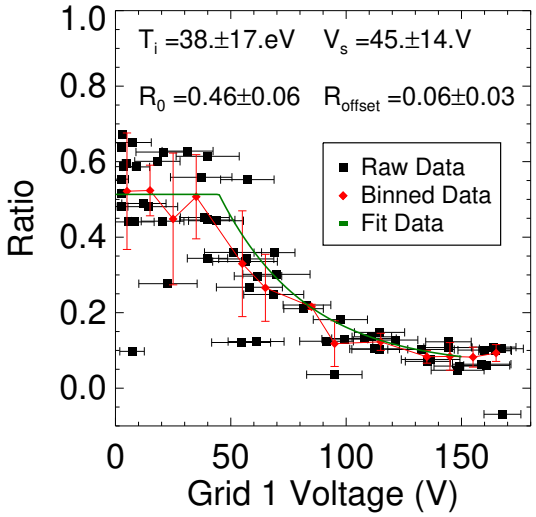

Figure 5. A typical graph of normalised ion current versus grid 1 voltage for filaments in a low density I_p=0.6MA discharge at a distance from 0 to 1cm from the separatrix. The red diamonds were obtained by binning the raw data into containers of approximately 10V width. The green line was fitted to the binned data using equation (3) and resulted in the fitting parameters shown on the graph.

filament ions are in thermal equilibrium, the ion temperature (T_i) can be determined by fitting a graph of normalised ion current density versus grid 1 voltage to the equation

$$R = R_0 \exp\left[-\frac{(V_{grid1} - V_s)}{T_i}\right] + R_{offset} \tag{3}$$

where T_i is in eV, R_0 is the ratio value when all ions reach the collector, V_{grid1} is the grid 1 voltage (in V), V_s is the potential of the sheath around the RFEA (in V) and R_{offset} is an offset value. A typical characteristic from a set of filaments is shown in figure 5 along with the values obtained by fitting equation (3). The data was obtained in a low density ($\bar{n}_e$=1x10^{19}m^{-3}) discharge with I_p=0.6MA at distances from 0 to 1cm from the separatrix. Each data point in figure 5 was taken from an individual filament similar to that shown in figure 4. The exponential decay of the normalised collector current with increasing grid 1 voltage shows that it is reasonable to use a set of filaments, at a fixed distance from the separatrix, to obtain an average filament temperature.

2.1. Effect of Grid 1 Voltage Averaging

During a filament, the voltage of grid 1 will vary as it is being swept. For characteristics and fitting, the average value of the grid 1 voltage in a 50μs period centred around the filament peak on the slit plate current trace was used. To assess the extent of grid 1 voltage averaging on the fitted ion temperature, a simulated set of filament data was produced using equation (3), with T_i=10eV, V_s=20V, R_0=1.0 and R_{offset}=0. This data is shown as the black squares in figure 6. During a 50μs period the grid 1 voltage

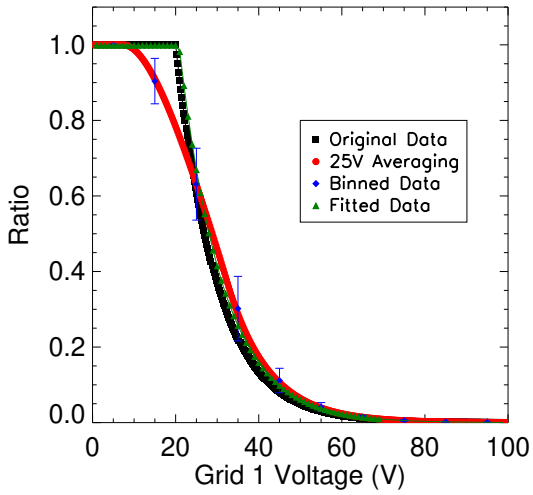

Figure 6. Assessing the effects of using an average grid 1 voltage value on the fitted T_i. The black squares show simulated raw data obtained using equation (3) with a 10eV ion temperature. The red circles show data obtained by averaging the raw data over 25V. The blue diamonds were obtained by binning the averaged data in bins of 10V width. The green triangles were obtained by fitting the binned data using equation (3) and gave a T_i of 10.4± 0.4eV.

changed by approximately 25V. To simulate this effect, the original data in figure 6 was averaged over 25V (shown as red circles) and equation (3) fitted to this data after it had been binned in containers with a width of approximately 10V. The resulting fit is shown by the green line and gave a temperature of 10.4± 0.4eV. This result indicates that the effect of grid 1 voltage sweeping is not significant for this work.

3. Results and Analysis

3.1. Midplane Measurements

Measurements were made in low ($\bar{n}_e$=1x10$^{19}m^{-3}$) and high density ($\bar{n}_e$=2x10^{19}m^{-3}) L-mode plasmas with plasma currents of 0.4 and 0.6MA. Figure 7 compares the area under filament peaks measured on the slit plate, in a 50μs window centred on the peak, in a low (#29464) and high density (#29469) I_p=0.6 MA shot. For both densities the raw data was binned with respect to distance from the separatrix and the binned data was then fitted with exponential functions for the near and far SOL. For the low density shot this gave exponential decay lengths of $\lambda_{near} = 6 \pm 2mm$ and $\lambda_{far} = 21 \pm 5mm$. For the high density shot the fitted decay lengths were $\lambda_{near} = 11 \pm 5mm$ and $\lambda_{far} = 54 \pm 15mm$. For both the low and high density cases, there is a rapid fall off in the filament ion saturation current in the first centimetre of the SOL followed by a more gradual decrease in the far SOL. At high density, the far SOL decay length was larger indicating a more gradual

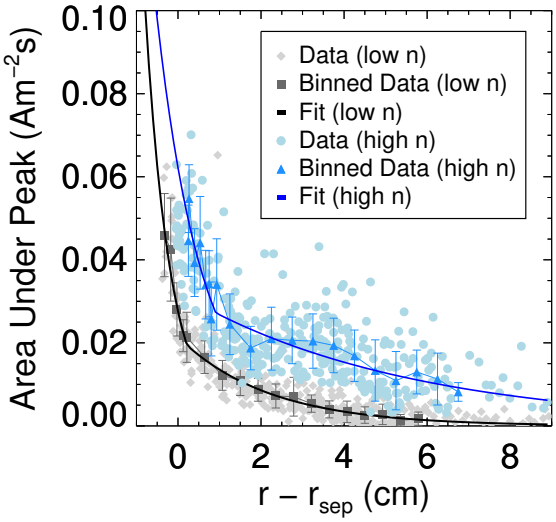

Figure 7. Area under slit plate peaks during filaments as a function of distance from the separatrix (r_{sep}). Filament data was taken from a low (29464) and high (29469) density, I_p=0.6MA L-mode shot. Exponential fitting to the near and far SOL of the binned data gave decay lengths of $\lambda_{near} = 6 \pm 2mm$ and $\lambda_{far} = 21 \pm 5mm$ for the low density shot and $\lambda_{near} = 11 \pm 5mm$ and $\lambda_{far} = 54 \pm 15mm$ for the high density shot.

fall off in saturation current compared to the low density case. This is a similar trend to that obtained from Langmuir probe measurements of inter-ELM filaments in MAST [6].

Figure 8 shows the large filament ion and electron temperatures measured in a 0.6MA low density plasma. The data is a weighted average from two identical shots (#29464 and #29465). The electron temperature was calculated from the sheath potential (V_s) obtained by fitting equation (3) to the data, assuming that $V_s \approx 3T_e$ [26]. From 0 to 4cm from the LCFS, the large filament ion temperature profile was relatively flat, ranging from 30 to 70eV. The large filament electron temperature profile was also relatively flat with a value of approximately 10eV which gave a T_i/T_e ratio of 3 to 7.

Figure 9 shows a comparison of large filament ion temperatures with background small filament ion and electron temperatures obtained in the low density L-mode shots. Background measurements were made using RFEA collector current data which was below the large filament detection threshold. From 0 to 1.5cm from the separatrix the background filament ion temperature ranged from 20 to 80eV which matches previous RFEA measurements made in similar L-mode plasmas [19] where T_i data included both large filaments and background plasma made up of small filaments. Over this region of the SOL, the large filament and background small filament ion temperatures were similar to each other. From 1.5 to 2.5cm from the separatrix, the background T_i decreased to range from 5 to 40eV while the large filament T_i remained relatively constant from 40 to 70eV. The large filament T_i remained approximately 2 to 3 times higher than

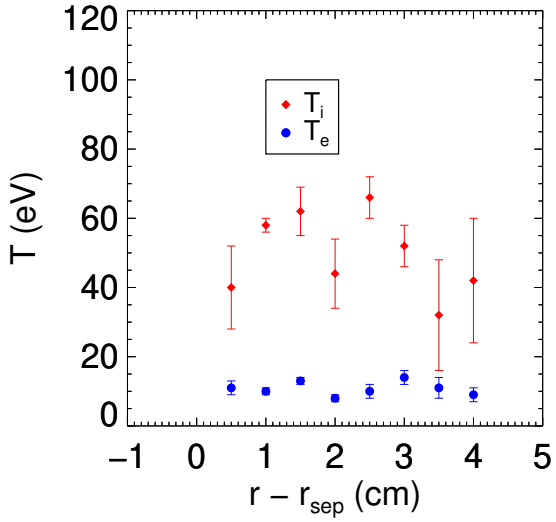

Figure 8. Comparison of ion (T_i) and electron (T_e) temperatures during large filaments in two repeat low density L-mode shots (29464 and 29465).

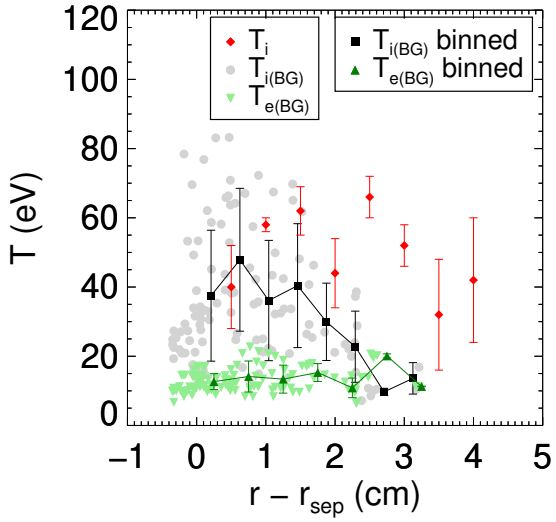

Figure 9. Comparison of background (BG) ion (T_i) and electron (T_e) temperatures with large filament ion temperatures in two repeat low density L-mode shots (29464 and 29465).

the background T_i into the far SOL from 2 to 4cm from the separatrix. This result is comparable to measurements made in AUG [18] which found that at a distance of 21mm from the separatrix the filament T_i was approximately 3 to 4 times higher than the background T_i.

From 0 to 3cm from the separatrix, the background electron temperature remained relatively constant from 10 to 20eV which was approximately 2 to 5 times smaller

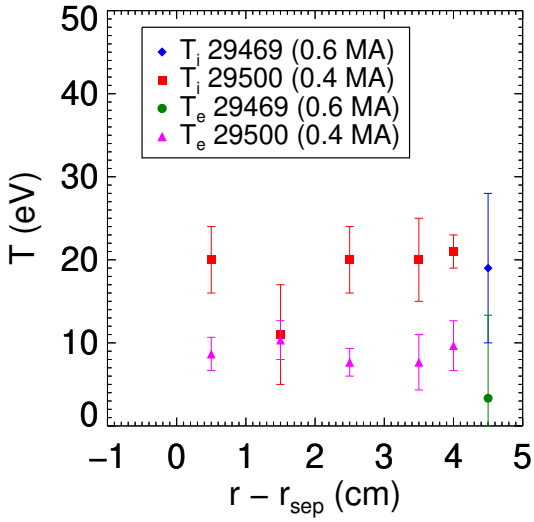

Figure 10. Comparison of ion (T_i) and electron (T_e) temperatures during large filaments in high density L-mode shots (29469 and 29500).

than the background ion temperature. At the separatrix, these results matched those obtained from Thomson laser scattering in a similar L-mode plasma [19]. Comparison with large filament T_e measurements in figure 8 show that the filament and background plasma T_e values are approximately the same from 0 to 3cm from the separatrix.

Figure 10 shows a comparison between the ion and electron temperatures measured in large filaments in high density L-mode shots with plasma currents of 0.4MA and 0.6MA. Only 1 point was obtained in a 0.6MA shot due to the failure of the slit plate power supply. From 0 to 5cm from the separatrix, the large filament ion temperature was relatively constant with a value of 5 to 20eV. The filament electron temperature was also relatively constant over the same distance with a value of 5 to 10eV which gave a T_i/T_e ratio between 1 and 4. Compared to the low density data in figure 8, the large filament ion temperatures in the high density shots were approximately 2 to 5 times smaller while the electron temperatures in the high density shots were approximately the same as those obtained from the low density data.

Figure 11 shows a comparison between large filament and background small filament ion and electron temperatures measured in the high density shots. From 0 to 0.5cm from the separatrix the background filament ion temperatures ranged from 5 to 40eV which matched previous RFEA measurements of similar density discharges [19] where large filament and background plasma data were not separated. From 0.5 to 1cm from the separatrix, the background filament ion temperature decreased to around 5 to 20eV and remained relatively constant out to a distance of 5cm from the separatrix. For the high density shots, the large filament T_i values were approximately the same as the small background filament T_i close to the separatrix but were approximately twice the background small filament values in the far SOL. The background filament electron

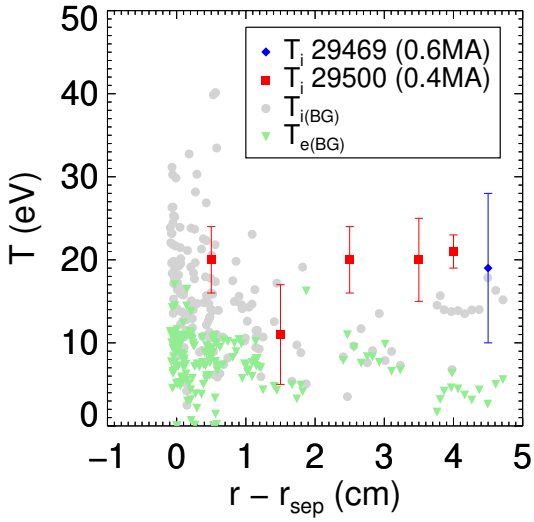

Figure 11. Comparison of background (BG) and large filament ion temperatures in high density L-mode shots 29469 (I_p=0.6MA) and 29500 (I_p=0.4MA).

temperature was relatively constant across the SOL with values between 5 to 10eV which gave a T_i/T_e ratio of 1 to 2 for the background plasma. At the separatrix, the T_e values matched measurements made in similar discharges using Thomson laser scattering [19].

3.2. Divertor Measurements

Ion temperature measurements were made at the lower divertor target in a low density I_p = 0.6 MA shot (#30357) which had the same conditions as used for the midplane measurements and in the same high density I_p = 0.4 MA shot (#29500) as used for midplane measurements. Divertor measurements in the low density scenario were made using a fast sweep technique (FST) where the grid 1 voltage was swept at a faster frequency of 20kHz [27]. This allowed each filament to be measured by several sweeps, each lasting 50 μs. Measurements from the low density discharge are shown in figure 12 along with a line showing calculations of a model of conductive and convective cooling which is discussed in section 3.3. It can be seen that the large filament temperatures are generally higher than T_i measured in the background SOL plasma, consistent with the midplane measurements, where large filaments were hotter than the background. Both the large filament and background ion temperatures decrease with increasing distance from the separatrix.

The high density discharge measurements were made using the same method as that used at the midplane. Large filaments were only measured at one radial location when mapped to the midplane of ΔR^{up}_{LCFS} = 4.3cm. In figure 13, this measurement is compared to the background T_i measured once the large filament signals had been removed. There is a clear difference between the background T_i and the single radially averaged filament measurement showing that, as with the midplane measurements, hot

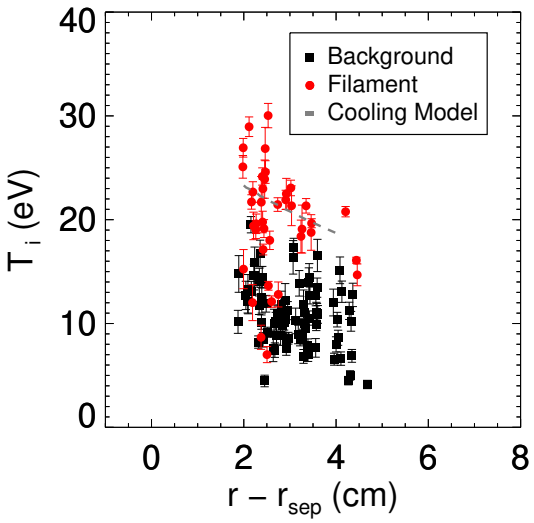

Figure 12. Low density measurements of large filament and background T_i measured by the target RFEA, mapped to the midplane. The grey dashed line shows the results of a calculation of cooling of filament ions due to conduction and convection as they move radially outward.

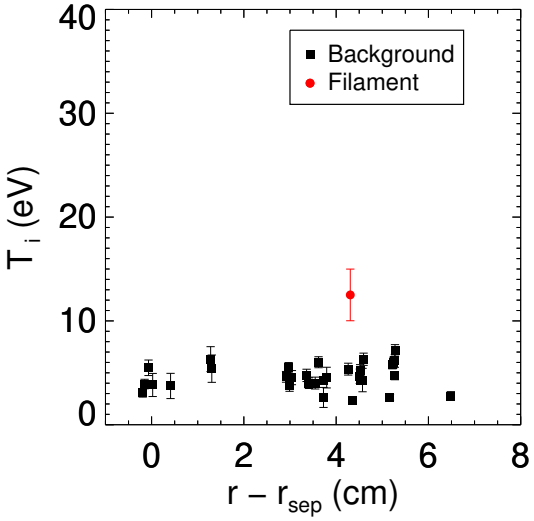

Figure 13. High density measurements of large filament and background T_i measured by the target RFEA, mapped to the midplane.

ions can reach far into the SOL by filamentary transport. At high densities, the midplane large filament T_i values were lower than at low densities and this is also seen at the divertor. As only one set of measurements was possible at the divertor at high density it is difficult to compare these results to the low density divertor case.

3.3. Discussion

The results from this work have shown that large filaments propagate into the far SOL in both low and high density L-mode plasmas with relatively flat ion temperature profiles that are hotter than the smaller background filaments. From 0 to 1.5cm from the separatrix, the large and small background filaments have similar ion temperatures while from 1.5 to 5cm from the separatrix, the large filaments remain 2 to 3 times hotter than the background filaments in the low density shots and around 2 times hotter than the background filaments in the high density shots. In this section we address the questions of whether it is possible for filaments to carry high energy ions into the far SOL and why the small background filaments are cooler than the large filaments.

For filaments to carry high energy ions into the far SOL the filament propagation time across the SOL must be less than the time required for filament ions to equilibrate in temperature with SOL electrons and to cool through conduction and convection. The filament propagation time across the SOL (τ_r) is given by

$$\tau_r = \frac{w}{v_f} \tag{4}$$

where w is the SOL width in metres (m) and v_f is the filament radial speed in metres per second (ms^{-1}). Fast camera measurements of L-mode plasmas in MAST have recorded filaments with radial extents of 5 to 10cm and radial velocities of 0.5 to 1.5kms^{-1} [5]. If a v_f of 1kms^{-1} and a SOL width of 3cm is assumed then the propagation time is τ_r=30μs.

Ion cooling occurs due to collisions of ions with electrons and due to conduction and convection along magnetic field lines. Due to their smaller mass, electrons have a higher velocity than ions of the same energy which results in electrons being lost more rapidly from the plasma, leaving only cold electrons as shown in the measurements made at both low and high densities in this work. The energy transferred during ion-electron collisions (W_i) can be determined using the Braginskii plasma fluid equations [28] and is given by

$$W_i = \frac{3n}{\tau_e}\frac{m_e}{m_i}\left(T_e - T_i\right) \tag{5}$$

where n is the number density in particles per cubic metre, m_e and m_i are the electron and ion masses in kilograms, T_e and T_i are the electron and ion temperatures in Joules and τ_e is the electron collision time in seconds. The electron collision time is given by

$$\tau_e = \frac{6\sqrt{2}\pi^{3/2}\epsilon_0^2\sqrt{m_e}T_e^{3/2}}{ne^4\ln\Lambda} \tag{6}$$

where $\ln\Lambda$ is given approximately by

$$\ln\Lambda \approx 6.6 - 0.5\ln\left(\frac{n}{10^{20}}\right) + 1.5\ln\left(\frac{T_e}{e}\right) \tag{7}$$

From equation (5), the timescale for ions to equilibrate in temperature with electrons (τ_{ie}) is of the order of $(m_i/m_e)\,\tau_e$. For typical MAST separatrix conditions of T_e=50eV and n=10^{19}m^{-3} this gives a value of $\tau_{ie} \approx 1000\mu$s.

The timescale for energy loss via conduction (τ_{cond}) can be estimated by considering conduction along a flux tube connecting the midplane to the divertor. The heat flux due to conduction (q_{cond}) [28] is given by

$$q_{cond} = \left(\frac{3.9 n \tau_i T_i}{m_i}\right) \frac{dT_i}{dx} \tag{8}$$

where τ_i is the ion collision time which is given by

$$\tau_i = \frac{12\pi^{3/2}\epsilon_0^2 \sqrt{m_i} T_i^{3/2}}{n e^4 \ln \Lambda} \tag{9}$$

Substitution of (9) into (8) gives

$$q_{cond} = \left(\frac{46.8 T_i^{5/2} \pi^{3/2} \epsilon_0^2}{m_i^{1/2} e^4 \ln \Lambda}\right) \frac{dT_i}{dx} \tag{10}$$

The total energy (U_T) of the flux tube is given by

$$U_T = \frac{3}{2}\left(nAd\right)\left(eT_i\right) - q_{cond} A t \tag{11}$$

where A is the area of the flux tube end through which conduction occurs in m^2, d is the flux tube length in metres and t is a time length in seconds. If flux expansion is ignored, for a circular cross section flux tube with a radius of 5mm and length of 10m, a density of $1\mathrm{x}10^{19}\mathrm{m}^{-3}$, an initial ion temperature of 100eV at the midplane and a fixed ion temperature of 1eV at the divertor, the time required for the midplane ion temperature to decrease to $1/e$ of its original value is $\tau_{cond} \approx 200\mu$s. These temperature values represent an extreme case that would give the largest possible temperature gradient and shortest possible conduction energy loss time.

The timescale for ion energy loss due to convection along a flux tube connecting the midplane to the divertor (τ_{conv}) can be estimated by assuming that the ions travel along the field line at the sound speed (c_s) [26]. The time taken for ions to travel down a field line of length L is

$$\tau_{conv} = \frac{L}{c_s} = L\left(\frac{m_i}{e\left(T_e + T_i\right)}\right)^{1/2} \tag{12}$$

If a ratio of T_i=2T_e [19] with T_i=50eV is taken with L=10m then the conduction time will be 167μs. These estimates show that $\tau_r(30\mu s) < \tau_{conv}(167\mu s) < \tau_{cond}(200\mu s) < \tau_{ie}(1000\mu s)$ and verify that the ions in filaments can carry energy radially outward faster than energy is transported along magnetic field lines or transferred through ion-electron collisions.

While these calculations show that filament ions can remain hot out into the far SOL, they do not explain why the smaller background filaments were cooler than the larger filaments in the far SOL. A reason for this may be that the smaller background filaments have a lower radial velocity compared to the larger filaments allowing them to lose more of their energy and particles closer to the separatrix. A drift interchange Alfvén fluid model for warm ions [29] has shown that filament radial velocity (v_f) scales with filament size (δ_f). For the filaments in this work, which had radial extents less

than 10cm, the model predicts that v_f will be proportional to δ_f^2 which would result in smaller filaments travelling more slowly than larger filaments in the SOL.

The presence of more small filaments in the far SOL of the high density shots in figure 11 compared to the low density shots in figure 9 is attributed to the increased density giving more plasma in the far SOL. As the smaller filaments have less particles than the larger filaments, at low density it is possible that they drop below the detection threshold of the RFEA in the far SOL.

Compared to the low density data in figure 8, the filament ion temperatures in the high density shots in figure 11 were lower and much closer to the electron temperature with a relatively flat profile across the SOL. This is attributed to the lower core ion and electron temperatures in the high density shots compared to those of low density. Measurements in a number of tokamaks including Alcator C-Mod [30] and ASDEX-Upgrade [31] have shown the formation of a flat density profile in the far SOL as core density is increased beyond a Greenwald fraction of approximately 0.5. The measurements in this work covered a Greenwald fraction from 0.22 to 0.67 and show a significant drop in large filament ion temperature between the lower and higher Greenwald fractions.

Compared to the midplane, at the divertor both the large filament and background smaller filaments were cooler. This is attributed to energy loss from ion-electron collisions and convection and conduction along the field lines. For the larger filaments, a decrease in temperature is also seen across the SOL at the target. This cooling may also be caused by the conduction, convection and ion-electron collisions mentioned previously. Ions at the target closer to the separatrix would remain hotter as they have not travelled out as far and have not had enough time to cool compared to ions in the far SOL. A calculation showing the effect of cooling due to conduction and convection is shown in figure 12. In this calculation it was assumed that ions had a radial velocity of 1kms^{-1}, the plasma density was $1\text{x}10^{19}\text{m}^{-3}$ and the flux tube connecting the midplane to the divertor was 10m long with a radius of 5mm. Over the 20 μs it takes for ions to move radially outward by 2cm, the calculation shows that ions would be expected to cool by approximately 10eV which is a similar decrease to that seen in the experimental results. The smaller number of large filaments in the far SOL at the divertor compared to the midplane is attributed to the radial velocity of these large filaments convecting them away to the walls before they can reach the divertor target.

4. Conclusion

In this paper, RFEA probes were used to compare the temperature of ions and electrons in large filaments with background plasma composed of smaller filaments. At low densities, the large filament ion temperature profile at the midplane was relatively flat with a value of 20 to 70eV for distances from 0 to 4cm from the separatrix. For distances from 2 to 4cm from the separatrix, the large filament T_i was 2 to 3 times greater than the background ion temperature. A similar result was observed by the RFEA at the

divertor target. Calculations based on the Braginskii fluid equations show that the time required for filaments to propagate radially outwards from the separatrix is less than the time required for filaments to cool through ion-electron collisions or through conduction or convection along magnetic field lines thus allowing filament ions to maintain high temperatures into the far SOL. Based on the predictions of a warm ion fluid model, it is hypothesised that smaller background filaments are not seen in the far SOL due to their lower radial velocity compared to larger filaments which results in the draining of more of their energy and particles closer to the separatrix.

At the midplane, for distances from 0 to 2cm from the separatrix, the large filament and background ion temperatures were comparable to each other with the background ion temperature ranging from approximately 20 to 80eV. This indicates that within this region, the small filaments in the background plasma are of comparable temperature to the larger filaments which are able to propagate into the far SOL.

At higher densities, the large filament ion temperature profile from 0 to 5cm from the separatrix was relatively flat with a value of 10 to 20eV. From 0 to 1cm from the separatrix the large filament ion temperature was similar to the small background filament ion temperature but from 1 to 5cm from the separatrix the large filament ion temperature was approximately twice the background filament ion temperature.

Measurements have recently been made of the heat flux profile of L-mode filaments at the divertor in MAST using infrared thermography [32]. These measurements were made in an I_p=0.8MA plasma with 3.7 MW of neutral beam heating and showed that for distances from the separatrix greater than 5cm, the filaments carried an average of 0.14±0.1MW of power to the target. This showed that the total power carried by the filaments to the outer divertor was small compared to the total input power. The RFEA measurements reported in this paper provide a further insight into ions in these large filaments. While the fall off length for ion saturation current (and hence plasma density and temperature) may be of the order of 10 to 20mm, the large filaments transport ions of relatively high temperature into the far SOL 2 to 4cm from the separatrix. This shows that in the far SOL, large filaments have low densities of high energy ions which carry small amounts of power into the far SOL. As the energy of ions impinging on a surface greatly affects the sputtering yield, this result has important implications for the design of plasma facing components which may release material back into the SOL when struck by these large filaments.

Acknowledgements

The authors would like to acknowledge the technical support of Nigel Thomas-Davies, Robert Stephen, Stuart Bray and Robert Gaffka in the design and operation of the RFEA probes and Andrew Kirk, Hendrik Meyer and Fulvio Militello for feedback on the paper content.

This work has been carried out within the framework of the EUROFusion Consortium and has received funding from the EURATOM research and training

programme 2014-2018 under grant agreement No 633053 and from the RCUK Energy Programme [grant number EP/I501045]. To obtain further information on the data and models underlying this paper please contact PublicationsManager@ccfe.ac.uk. The views and opinions expressed herein do not necessarily reflect those of the European Commission.

References

[1] S. I. Krasheninnikov, D. A. D'ippolito, and J. R. Myra. Recent theoretical progress in understanding coherent structures in edge and SOL turbulence. *J. Plasma Phys.*, 74(05):679–717, October 2008.

[2] S. J. Zweben, J. A. Boedo, O. Grulke, C. Hidalgo, B. LaBombard, R. J. Maqueda, P. Scarin, and J. L. Terry. Edge turbulence measurements in toroidal fusion devices. *Plasma Phys. Control. Fusion*, 49(7):S1, 2007.

[3] D. A. DIppolito, J. R. Myra, and S. J. Zweben. Convective transport by intermittent blob-filaments: Comparison of theory and experiment. *Phys. Plasmas*, 18(6):060501, 2011.

[4] J. A. Boedo. Edge turbulence and SOL transport in tokamaks. *J. Nucl. Mater.*, 390-391:29–37, 2009.

[5] B. D. Dudson, N. Ben Ayed, A. Kirk, H. R. Wilson, G. Counsell, X. Xu, M. Umansky, P. B. Snyder, B. LLoyd, and the MAST team. Experiments and simulation of edge turbulence and filaments in MAST. *Plasma Phys. Control. Fusion*, 50(12):124012, 2008.

[6] N. Ben Ayed, A. Kirk, B. Dudson, S. Tallents, R. G. L. Vann, H. R. Wilson, and the MAST Team. Inter-ELM filaments and turbulent transport in the Mega-Amp Spherical Tokamak. *Plasma Phys. Control. Fusion*, 51(3):035016, 2009.

[7] O. Grulke, J. L. Terry, I. Cziegler, B. LaBombard, and O. E. Garcia. Experimental investigation of the parallel structure of fluctuations in the scrape-off layer of Alcator C-Mod. *Nucl. Fusion*, 54(4):043012, 2014.

[8] H. W. Müller, J. Adamek, R. Cavazzana, G. D. Conway, C. Fuchs, J. P. Gunn, A. Herrmann, J. Horaček, C. Ionita, A. Kallenbach, M. Kočan, M. Maraschek, C. Maszl, F. Mehlmann, B. Nold, M. Peterka, V. Rohde, J. Schweinzer, R. Schrittwieser, N. Vianello, E. Wolfrum, M. Zuin, and the ASDEX Upgrade Team. Latest investigations on fluctuations, ELM filaments and turbulent transport in the SOL of ASDEX Upgrade. *Nucl. Fusion*, 51(7):073023, 2011.

[9] D. L. Rudakov, J. A. Boedo, J. H. Yu, N. H. Brooks, M. E. Fenstermacher, M. Groth, E. M. Hollmann, C. J. Lasnier, A. G. McLean, R. A. Moyer, P.C. Stangeby, G. R. Tynan, W. R. Wampler, J. G. Watkins, W. P. West, C. P. C. Wong, R. J. Bastasz, D. Buchenauer, and J. Whaley. Plasma interactions with the outboard chamber wall in DIII-D. *J. Nucl. Mater.*, 390-391:785–788, 2009.

[10] R. A. Pitts, P. Andrew, G. Arnoux, T. Eich, W. Fundamenski, A. Huber, C. Silva, D. Tskhakaya, and JET EFDA Contributors. ELM transport in the JET scrape-off layer. *Nucl. Fusion*, 47(11):1437, 2007.

[11] C. Silva, B. Goncalves, C. Hidalgo, M. A. Pedrosa, W. Fundamenski, M. Stamp, R. A. Pitts, and JET-EFDA contributors. Intermittent transport in the JET far-SOL. *J. Nucl. Mater.*, 390-391:355–358, 2009.

[12] F. Militello, P. Tamain, W. Fundamenski, A. Kirk, V. Naulin, A. H. Nielsen, and the MAST team. Experimental and numerical characterization of the turbulence in the scrape-off layer of MAST. *Plasma Phys. Control. Fusion*, 55(2):025005, 2013.

[13] J. A. Boedo, J. R. Myra, S. Zweben, R. Maingi, R. J. Maqueda, V. A. Soukhanovskii, J. W. Ahn, J. Canik, N. Crocker, D. A. D'Ippolito, R. Bell, H. Kugel, B. Leblanc, L. A. Roquemore, D. L. Rudakov, and NSTX Team. Edge transport studies in the edge and scrape-off layer of

the National Spherical Torus Experiment with Langmuir probes. *Phys. Plasmas*, 21(4):042309, 2014.

[14] O. E. Garcia, R. A. Pitts, J. Horacek, A. H. Nielsen, W. Fundamenski, J. P. Graves, V. Naulin, and J. Juul Rasmussen. Turbulent transport in the TCV SOL. *J. Nucl. Mater.*, 363-365:575–580, 2007.

[15] P. Tamain, M. Kočan, J. Gunn, A. Kirk, J.-Y. Pascal, and M. Price. Ion energy measurements in the scrape-off layer of MAST using a Retarding Field Analyzer. *J. Nucl. Mater.*, 415(1, Supplement):S1139 – S1142, 2011.

[16] R. A. Pitts, W. Fundamenski, S. K. Erents, Y. Andrew, A. Loarte, C. Silva, and JET-EFDA contributors. Far SOL ELM ion energies in JET. *Nucl. Fusion*, 46(1):82, 2006.

[17] M. Kočan, S. Y. Allan, S. Carpentier-Chouchana, P. de Marné, S. Elmore, T. Franke, J. P. Gunn, A. Herrmann, A. Kirk, M. Kubič, T. Lunt, H. W. Müller, R. A. Pitts, V. Rohde, and the ASDEX Upgrade Team. Ion energies and currents of type I and mitigated ELMs in the ASDEX Upgrade far scrape-off layer. *Nucl. Fusion*, 52(2):023016, 2012.

[18] M. Kočan, F. P. Gennrich, A. Kendl, H. W. Müller, and the ASDEX Upgrade Team. Ion temperature fluctuations in the ASDEX Upgrade scrape-off layer. *Plasma Phys. Control. Fusion*, 54(8):085009, 2012.

[19] S. Elmore, S. Y. Allan, A. Kirk, G. Fishpool, J. Harrison, P. Tamain, M. Kočan, R. Gaffka, R. Stephen, J. W. Bradley, and the MAST Team. Upstream and divertor ion temperature measurements on MAST by retarding field energy analyser. *Plasma Phys. Control. Fusion*, 54(6):065001, 2012.

[20] G. Fishpool, J. Canik, G. Cunningham, J. Harrison, I. Katramados, A. Kirk, M. Kovari, H. Meyer, and R. Scannell. MAST-upgrade divertor facility and assessing performance of long-legged divertors. *J. Nucl. Mater.*, 438, Supplement:S356–S359, 2013.

[21] J. R. Harrison, G. M. Fishpool, and A. Kirk. L-mode and inter-ELM divertor particle and heat flux width scaling on MAST. *J. Nucl. Mater.*, 438, Supplement:S375–S378, 2013.

[22] H. Meyer, I. G. Abel, R. J. Akers, A. Allan, S. Y. Allan, L. C. Appel, O. Asunta, M. Barnes, N. C. Barratt, N. Ben Ayed, J. W. Bradley, J. Canik, P. Cahyna, M. Cecconello, C. D. Challis, I. T. Chapman, D. Ciric, G. Colyer, N. J. Conway, M. Cox, B. J. Crowley, S. C. Cowley, G. Cunningham, A. Danilov, A. Darke, M. F. M. De Bock, G. De Temmerman, R. O. Dendy, P. Denner, D. Dickinson, A. Y. Dnestrovsky, Y. Dnestrovsky, M. D. Driscoll, B. Dudson, D. Dunai, M. Dunstan, P. Dura, S. Elmore, A. R. Field, G. Fishpool, S. Freethy, W. Fundamenski, L. Garzotti, Y. C. Ghim, K. J. Gibson, M. P. Gryaznevich, J. Harrison, E. Havlí čková, N. C. Hawkes, W. W. Heidbrink, T. C. Hender, E. Highcock, D. Higgins, P. Hill, B. Hnat, M. J. Hole, J. Horáček, D. F. Howell, K. Imada, O. Jones, E. Kaveeva, D. Keeling, A. Kirk, M. Kočan, R. J. Lake, M. Lehnen, H. J. Leggate, Y. Liang, M. K. Lilley, S. W. Lisgo, Y. Q. Liu, B. Lloyd, G. P. Maddison, J. Mailloux, R. Martin, G. J. McArdle, K. G. McClements, B. McMillan, C. Michael, F. Militello, P. Molchanov, S. Mordijck, T. Morgan, A. W. Morris, D. G. Muir, E. Nardon, V. Naulin, G. Naylor, A. H. Nielsen, M. R. O'Brien, T. O'Gorman, S. Pamela, F. I. Parra, A. Patel, S. D. Pinches, M. N. Price, C. M. Roach, J. R. Robinson, M. Romanelli, V. Rozhansky, S. Saarelma, S. Sangaroon, A. Saveliev, R. Scannell, J. Seidl, S. E. Sharapov, A. A. Schekochihin, V. Shevchenko, S. Shibaev, D. Stork, J. Storrs, A. Sykes, G. J. Tallents, P. Tamain, D. Taylor, D. Temple, N. Thomas-Davies, A. Thornton, M. R. Turnyanskiy, M. Valovič, R. G. L. Vann, E. Verwichte, P. Voskoboynikov, G. Voss, S. E. V. Warder, H. R. Wilson, I. Wodniak, S. Zoletnik, R. Zagôrski, and the MAST and NBI Teams. Overview of physics results from MAST towards ITER/DEMO and the MAST Upgrade. *Nucl. Fusion*, 53(10):104008, 2013.

[23] Y. Yang, G. F. Counsell, and the MAST team. Observations with a mid-plane reciprocating probe in MAST. *J. Nucl. Mater.*, 313316:734–737, 2003.

[24] G. De Temmerman, M. Bacharis, J. Dowling, and S. Lisgo. Dust creation and transport in MAST. *Nucl. Fusion*, 50(10):105012, 2010.

[25] M. Kočan, A. Herrmann, H. W. Müller, V. Rohde, T. Eich, T. Bernert, S. Carpentier-Chouchana, J. P. Gunn, A. Kirk, R. A. Pitts, and the ASDEX Upgrade Team. First measurements of edge localized mode ion enegies in the ASDEX Upgrade far scrape off layer. *Plasma Phys. Control. Fusion*, 53:065002, 2011.

[26] P. C. Stangeby. *The Plasma Boundary of Magnetic Fusion Devices*. Plasma Physics Series. IOP Publishing Ltd, Bristol, United Kingdom, 2000.

[27] S. Elmore, S. Y. Allan, G. Fishpool, A. Kirk, M. Kočan, P. Tamain, A. J. Thornton, and the MAST Team. Scrape-off layer ion temperature measurements at the divertor target during type III and type I ELMs in MAST measured by RFEA. *Submitted*, 2015.

[28] S. I. Braginskii. Transport Processes in a Plasma. In M. A. Leontovich, editor, *Reviews of Plasma Physics*, volume 1, pages 205–311. Consultants Bureau, New York, 1965.

[29] P. Manz, D. Carralero, G. Birkenmeier, H. W. Müller, S. H. Müller, G. Fuchert, B. D. Scott, and U. Stroth. Filament velocity scaling laws for warm ions. *Phys. Plasmas*, 20(10):102307, October 2013.

[30] B. LaBombard, R. L. Boivin, M. Greenwald, J. Hughes, B. Lipschultz, D. Mossessian, C. S. Pitcher, J. L. Terry, S. J. Zweben, and Alcator Group. Particle transport in the scrape-off layer and its relationship to discharge density limit in Alcator C-Mod. *Physics of Plasmas (1994-present)*, 8(5):2107–2117, May 2001.

[31] D. Carralero, G. Birkenmeier, H. W. Müller, P. Manz, P. deMarne, S. H. Müller, F. Reimold, U. Stroth, M. Wischmeier, E. Wolfrum, and The ASDEX Upgrade Team. An experimental investigation of the high density transition of the scrape-off layer transport in ASDEX Upgrade. *Nuclear Fusion*, 54(12):123005, December 2014.

[32] A. J. Thornton, G. Fishpool, A. Kirk, the MAST Team, and the EUROfusion MST1 Team. The effect of L mode filaments on divertor heat flux profiles as measured by infrared thermography on MAST. *Plasma Physics and Controlled Fusion*, 57(11):115010, 2015.